Numerical Investigation of a Fuselage Boundary Layer Ingestion Propulsion Concept

Alaa A. Elmiligui[1], William J. Fredericks[2], Mark D. Guynn[3], and Richard L. Campbell[4]
NASA Langley Research Center, Hampton, VA, 23681, USA

In the present study, a numerical assessment of the performance of fuselage boundary layer ingestion (BLI) propulsion techniques was conducted. This study is an initial investigation into coupling the aerodynamics of the fuselage with a BLI propulsion system to determine if there is sufficient potential to warrant further investigation of this concept. Numerical simulations of flow around baseline, Boundary Layer Controlled (BLC), and propelled boundary layer controlled airships were performed. Computed results showed good agreement with wind tunnel data and previous numerical studies. Numerical simulations and sensitivity analysis were then conducted on four BLI configurations. The two design variables selected for the parametric study of the new configurations were the inlet area and the inlet to exit area ratio. Current results show that BLI propulsors may offer power savings of up to 85% over the baseline configuration. These interim results include the simplifying assumption that inlet ram drag is negligible and therefore likely overstate the reduction in power. It has been found that inlet ram drag is not negligible and should be included in future analysis.

Nomenclature

BLC	=	boundary layer control
BLI	=	boundary layer ingestion
CFD	=	computational fluid dynamics
C_D	=	force coefficient in the *x* direction
C_{DW}	=	wake drag coefficient
C_p	=	pressure coefficient
Cx	=	force coefficient in the *x* direction
Fx	=	*X* component of the resultant pressure force acting on the vehicle
g	=	suction slot width, in
L	=	reference length, in
log(r/r0)	=	L2-norm of the mean flow residue
log(tnu/tnu0)	=	L2-norm of the turbulence flux residue

[1] Research Engineer, Configuration Aerodynamics Branch, Mail Stop 499, AIAA senior member.
[2] Aerospace Engineer, Aeronautics Systems Analysis Branch, Mail Stop 442, Young Professional.
[3] Aerospace Engineer, Aeronautics Systems Analysis Branch, Mail Stop 442, AIAA senior member.
[4] Senior Research Engineer, Configuration Aerodynamics Branch, Mail Stop 499, AIAA Associate Fellow.

M_∞ = freestream Mach Number
$\dot{m}$ = mass flow rate, slugs/sec
Po_{jet} = jet total pressure/ freestream static pressure
P_∞ = freestream static pressure
Re_L = Reynolds number based on reference length
r = Radial distance, in
V = body volume, ft^3
U_∞ = freestream velocity, ft/sec
ρ_∞ = freestream density, slugs/ft^3

I. Introduction

The claim that a boundary layer ingestion (BLI) fuselage can move through the air with less power than a conventional fuselage with an isolated propulsor has been debated over the years. In theory, accelerating lower velocity air from the boundary layer back to freestream velocity increases the propulsive efficiency compared to accelerating freestream air to generate the same thrust. The resulting BLI engine thrust provides wake filling for the momentum deficit of the fuselage. The BLI propulsion systems also provide a favorable pressure gradient to maintain airflow attachment enabling a steeper pressure recovery on the tail cone and pressure thrust to be generated on the fuselage.

There are two "schools of thought" regarding BLI. The first is to energize the boundary layer to change the pressure distribution around the body which changes axial force. The second is to ingest the low momentum flow in the boundary layer and accelerate it back to free-stream velocity in order to achieve a higher propulsive efficiency. Clearly these two "schools of thought" are closely coupled and likely are competing technologies. In this study, the authors will investigate fuselage BLI as a technology to reduce the fuel consumption of aircraft.

The development of wake regeneration, with and without active boundary-layer control has been studied by several researchers with various degrees of success [1-18]. Cerreta [2] conducted an investigation of the drag of a boundary layer controlled (BLC) airship, referred to as the "Cerreta airship," in the 7- by 10-Foot Transonic Wind Tunnel at the David Taylor Model Basin. Results showed that a savings in drag of approximately 20% could be achieved compared to XZS2G-1 baseline airship. Goldschmied [4] showed that a propulsion power reduction of 50% could be achieved with an integrated, self-propelled wind-tunnel model, referred to as the Goldschmied Propulsor.

Peraudo [11] conducted a numerical investigation of the flow around the XZS2G-1 airship, the Cerreta BLC airship and the Goldschmied self propelled BLC airship. A brief description of all three airships will be given later in section III of this paper. This investigation provided the basis for the current study. In parallel, a wind tunnel test [15-17] and a computational fluid dynamics (CFD) study [18] of the Goldschmied propulsor were conducted at the California Polytechnic State University. The goal was to investigate and document the performance of the Goldschmied propulsor. In the present study, a numerical assessment of the performance of fuselage boundary ingestion propulsion techniques will be conducted. The flow around the XZS2G-1 airship, the Cerreta BLC airship, and the Goldschmied propulsor are computed and compared with previous numerical and wind tunnel data. TetrUSS [19] will be the numerical code used in the present study. TetrUSS was developed at NASA Langley Research Center and includes a model/surface grid preparation tool (GridTool), field grid generation software (VGRID, POSTGRID), and a computational flow solver (USM3D).

For many decades jet airliners have isolated the propulsion systems in nacelles in a manner to minimize the interaction with the aerodynamics of the airframe. There are many reasons for this ranging from the difficulty associated with a multi-disciplinary optimization of the propulsion system and the airframe aerodynamics, to ease of engine accessibility for maintenance. This study is an initial investigation into coupling the aerodynamics of the fuselage with a propulsion system in order to determine if there is sufficient potential to warrant further investigation of this topic.

The fuselage was selected as the part of the aircraft to apply BLI propulsion for three reasons. First, as technology improves, all parts of the aircraft except the fuselage reduce in size. With advances in aircraft technology the wing and tail wetted areas will get smaller in size. Generally, the fuselage will not reduce in size because the size of the fuselage is set by the payload and passengers. Second, fuselages have the largest aerodynamic reference length of any component on the aircraft and thus they build up the thickest boundary layers. They will, therefore, have the greatest potential improvement from BLI. Third, fuselages are approximately an axisymmetric shape meaning that an inlet slot around the circumference of the fuselage would provide a flow field into the propulsor that is distortion free in the tangential direction. The fan blades would have to be twisted differently from a uniform inlet flow, but the flow field is axisymmetric. For these reasons it was determined that a fuselage would be the best place to apply BLI technology.

The objective of this report is to validate the claim that a BLI fuselage can move through the air with less power than a conventional fuselage. This is a conceptual level study of the physics behind BLI in order to design fuselages that maximize their BLI benefit. The configurations considered in the study are axisymmetric. Angle-of-attack and sideslip angles are set to zero.

The organization of the paper is as follows: (1) A brief description of the numerical tools, grid generation, and boundary conditions used in the study, (2) Numerical simulation of flow around the XZS2G-1 airship, BLC airship, and Goldschmied propulsor along with discussion and comparison to wind tunnel data, (3) A design of experiment and sensitivity analysis for four BLI fuselages, (4) Results and discussion section followed by, (5) Summary and concluding remarks.

II. Computational Modeling

The NASA software system used in the computational analysis was the Tetrahedral Unstructured Software System (TetrUSS) [19]. TetrUSS was developed at NASA Langley Research Center and includes a model/surface grid preparation tool (GridTool) [20], field grid generation software (VGRID, POSTGRID) [21-22], and a computational flow solver (USM3D) [23-24]. The USM3D flow solver has internal software to calculate forces and moments. Additionally, the NASA LaRC-developed code USMC6 [25] was used to extract data from the computational domain. The computational grids, flow solvers, and the boundary conditions for USM3D are described below.

A. TetrUSS Computational Grids

All the test cases generated in this study were quasi two-dimensional axisymmetric bodies of revolution. The grids were a 5° slice with one cell in the circumferential direction. The grids extended in all three directions up to fifteen body lengths. The approximate number of grid cells was 250,000. Some guidelines for grid generation included the requirement for surface cell size to be small enough to resolve features and curvature of the different bodies of interest. Proper boundary layer spacing was used to ensure y+ remained less than or equal to 1 for the selected freestream Mach and Reynolds numbers.

The body surface definitions for the XZS2G-1 airship, the unpropelled Cerrata airship, and Goldshmied propulsor were supplied by Peraudo [11] in plot3d format. The original set of grids was generated by creating surface patches on the configuration in GridTool using a PLOT3D surface definition of the geometry. Sources were placed throughout the domain to cluster cells and accurately capture configuration characteristics. The output from GridTool was used to automatically generate the computational domain with the VGRID unstructured grid generation software. VGRID uses an Advancing Layers Method to generate thin layers of unstructured tetrahedral cells in the viscous boundary layer, and an Advancing Front Method to populate the volume mesh in an orderly fashion. POSTGRID was used to close the grid by filling in any gaps that remain from VGRID. POSTGRID is automated to carefully remove a few cells surrounding any gaps in the grid and precisely fill the cavity with the required tetrahedral cells. In the present study, all the configurations are axisymmetric body of revolutions hence the authors decided to look for other avenues of generating the grids. The process had to be automated and generate good quality grids compatible with USM3D. An existing grid-extrusion code (Q2D) [25] was selected for this process. The original Q2D generated quasi-2D, one cell wide unstructured grids around airfoils. The authors modified Q2D to generate 2-D axisymmetric grids for axisymmetric bodies. Q2D still uses VGRID to generate a 2-D unstructured grid, and then prisms are extruded from the triangular faces in the circumferential direction from this symmetry plane. The prisms are then split into tetrahedral cells.

The current version of Q2D can now generate grids for airfoils as well as circular inlets and nozzles. The grid generation process is scripted, and generates grids within the order of seconds.

B. TetrUSS Flow Solver, USM3D

The flow solver for the TetrUSS software package is USM3D. USM3D is a tetrahedral cell-centered, finite volume Euler and Navier-Stokes (N-S) method. The USM3D flow solver has a variety of options for solving the flow equations and several turbulence models for closure of the N-S equations [26]. A script program was used to automatically setup input parameters for choosing the proper flux scheme and CFL numbers based on the desired Mach number for each case. For the current study, Roe's flux difference splitting scheme was used and CFL_{max} was set to 50. For the present study, at the start of a new solution, the USM3D code ran 10,000 iterations with first order spatial accuracy, and then the code automatically switched to second order spatial accuracy. Two turbulence models were investigated in this study, the Spalart–Allmaras (SA) model [27] and the shear stress transport (SST) model [28]. The SA turbulence model, which is a one equation model for turbulent viscosity, was the default turbulence model used. A limited number of cases were computed using the SST model to evaluate the effect of turbulence models on the numerical solution of BLI configurations. Details of the implementation of the turbulence models within USM3D can be found in Ref. [27].

C. Initial and Boundary Conditions

The characteristic inflow and outflow boundary condition (BC) was used along the far field, lateral faces of the outer domain for all test cases. The no-slip viscous BC was used on all solid surfaces. For the suction slot of the Cerrata BLC configuration, a sink boundary condition was used. The USM3D jet BC was used to model the jet exit and inlet planes for all BLI configurations. The jet outflow boundary condition is determined through user-prescribed values for total pressure, and total temperature conditions. The inlet-plane flow is determined automatically in USM3D through a mass flux balance with the jet flow by adjusting the average

back pressure on the inlet face. By using an average back pressure, any distortion on the inflow plane is maintained while the mass flux is balanced. Details of the implementation of the sink and jet BCs can be found in Ref. [30]. The sink BC within USM3D is identified as BC 111. The intake jet BC is 101, and the jet exit BC is 102.

III. Numerical Validation of Boundary Layer Ingestion Geometries

At the onset of this study, numerical simulations of the flow around the XZS2G-1 Airship, the Cerrata BLC Airship, and the propelled BLC "Goldchmied propulsor" Airship were conducted. The goals were to develop a better understating of the physics behind the BLI system; to validate the computational tools that would be used in the parametric study; and to compare numerical results from the current study with numerical results of reference [11] and wind tunnel data [2-4].

A. XZS2G-1 Airship

The XZS2G-1 airship is an axisymmetric body of revolution. Cerreta [2] conducted a wind tunnel test of the flow around the airship. A schematic of the XZS2G-1 airship is shown in Figure 1. XZS2G-1 airship surface definition was provided by reference [11]. Figure 2 shows a planar cut illustrating the grid distribution for a XZS2G-1 airship. Numerical simulations of the flow around the airship were conducted for a free-stream Mach number of 0.13 and 0.25, corresponding to Reynolds number of 4.60 million and 8.57 million respectively. The Reynolds numbers were based on the airship reference length of 58.5 inches. The SA turbulence model and SST turbulence model were used to model turbulence. The grid was a 5° slice with one cell in the circumferential direction and had 168,704 cells. In the wind tunnel test, a wake rake located approximately 3 feet downstream of the model was used to measure the total-head deficit and static pressure in the wake. The wake drag coefficient, $C_{DW,}$ was computed following Ref. [30] as:

$$C_{DW} = \frac{8\,\pi}{\rho_\infty U_\infty^2 V^{\frac{2}{3}}} \int_0^{r^*} \left| \sqrt{0.5\,\rho_\infty U(r)^2} \left(\sqrt{0.5 \rho_\infty U_\infty^2} - \sqrt{0.5\,\rho_\infty U(r)^2 + P(r) - P_\infty} \right) \right| \tag{1}$$

The coefficient of drag, C_D, is also computed internally by USM3D and is the sum of the skin friction and pressure drag. Table 1 shows comparison of the computed wake drag coefficient with numerical results of reference [11] and wind tunnel data [2]. The current results show good agreement with both numerical results and wind tunnel data. The C_D as computed by SA and SST turbulence models bracketed the wind tunnel data.

Table 1. Wake Drag Coefficient Results for the XZS2G-1 Airship

Mach Number	Reynolds Number (million)	Turbulence Model	WT Data [2]	Numerical Results [11]	Present Numerical Results (USM3D)
0.13	4.65	SA	0.0284	0.0243	0.0231
0.13	4.65	SST	0.0284	0.0242	0.0299
0.25	8.57	SA	0.0267	NA	0.0211
0.25	8.57	SST	0.0267	NA	0.0267

B. Boundary Layer Control Airship "Cerreta Airship"

The second configuration tested was the Cerreta BLC airship. The BLC airship is an axisymmetric body of revolution. A schematic of the BLC is shown in Figure 3. Cerreta conducted an extensive study on the BLC airship in the 7-by-10-ft Transonic Wind Tunnel at the David Taylor Model Basin [2]. Numerical simulations for the flow around the BLC airship were conducted for a free-stream Mach number of 0.29 corresponding to Reynolds number of 10.2 million based on the airship reference length of 58.5 inches. The surface definition for the BLC airship was provided by Ref. [11]. The suction gap was 0.71 inches wide and started at an axial location equal to 48.68 inches from model leading edge. The red band in Figure 3 illustrates the location of the suction gap. The test conditions and slot width were selected to match wind tunnel data. Figure 4 shows convergence history for the BLC airship in free air using the SA turbulence model. Figure 5 shows the Mach contours of the flow around the tail of the BLC airship with the streamlines superimposed for a freestream Mach number of 0.29. Figure 5a shows the flow around BLC airship when no suction was applied at the suction gap. The flow separates at the rear of BLC airship due to the thickening of the boundary layer and the sharp change of slope. The red arrow in Figure 5a points to the separation bubble. Applying a suction rate of 0.07 lb-sec/ft caused the flow to re-attach as shown in Figure 5b. Table 2 shows a comparison between computed wake drag coefficient using USM3D with the SA turbulence model, numerical results [11], and wind tunnel data [2]. Applying suction resulted in a significant reduction of the wake drag as computed by equation (1). The coefficient of pressure, C_p, on the surface of the BLC airship is shown in Figure 6. The black line with circles is C_p for the simulation with no suction. The blue line with squares is the C_p when suction was applied at a rate of 0.07 lb-sec/ft. There is an abrupt increase in the C_p across the suction slot. The suction results in the attachment of the flow on the trailing end of the airship as shown in Figure 5b. The present C_{DW} results using the SA turbulence model compared well with numerical results [11] for the no suction case and for the mass flow rate of 0.07 lb_f-sec/ft suction case. The present numerical results for the suction case are also in excellent agreement with wind tunnel data [2]. However for no suction case, the present C_{DW} results and numerical results of Ref. [11] do not agree with the wind tunnel C_{DW} of 0.0558. The authors of reference [11] postulated that the wind tunnel C_{DW} is a misprint. The authors concur with the misprint assumption especially that suction data agrees well with the experimental data.

Table 2. Wake Drag Coefficient Results for the Boundary Layer Control Airship at M_∞=0.21

Mass flow rate (lb_f-sec/ft)	WT Data Ref. [2]	Numerical Results Ref. [11]	Present Results USM3D – SA
No suction	0.0558	0.0307	0.02907
0.07	0.0054	0.0053	0.0054

C. Goldschmied Propulsor

The third configuration tested was the Goldschmied propulsor [4]. A schematic of the airship is shown in Figure 7. The surface definition for the Goldschmied propulsor was provided by Ref. [11]. Numerical simulations were conducted for a free-stream Mach number of 0.21 corresponding to a Reynolds number of 6.7 million based on an airship reference length of 53.6 inches. The suction gap was 0.87 in wide and started at an axial location equal to 48.68 inches

from model leading edge. The front part of the Goldschmied propulsor airship is the same as the one used by Cerrata [2]. The test conditions and slot width were selected to match wind tunnel data. Figure 8 shows grid distribution in the vicinity of the inlet slot while Figure 9 shows the grid distribution around the jet exit. The region between the inlet slot and jet exit boundary contains no grid, however the mass flux is conserved between the two planes. Table 3 shows a comparison between computed wake drag coefficient, C_{DW}, wind tunnel (WT) data [4] and numerical results [11] for the unpropelled Goldschmied airship at M_∞ = 0.21. The present numerical results for the unpropelled Goldschmied airship are in good agreement with wind tunnel data [4] and numerical results [11].

Table 3. Wake Drag Coefficient Results for unpropelled Goldschmied Propulsor at M_∞=0.21

Goldschmied WT [4]	Numerical Results [11]	Present Results USM3D – SA
0.034	0.03	0.032

Figure 10 shows the Mach contours of the flow around the tail of the Goldshmied airship with the streamlines superimposed for a Mach number of 0.21 and for Po_{jet}/P_∞ of 1.02. The propulsor total pressure, Po_{jet}/P_∞, was initially set equal to 1.02 to match the value used in the wind tunnel study. However, the streamlines near the rear of the airship show that the flow was still separated. The arrow in Figure 10 points to the separation bubble. Po_{jet}/P_∞ was increased until C_{DW} was equal to zero. New values for Po_{jet}/P_∞ were found by the following recurrence relation:

$$Po_{jet_{k+1}} = Po_k - \frac{\left(C_{D_k} * \left[Po_{jet_{k-1}} - Po_{jet_k}\right]\right)}{\left[C_{D_{k-1}} - C_{D_k}\right]} \quad (2)$$

Figure 11 shows Mach contours with streamlines superimposed for a freestream Mach number of 0.21 and Po_{jet}/P_∞ = 1.05. The flow is now fully attached and the wake drag coefficient, C_{DW}, is equal to zero. Table 4 shows a comparison of the computed results, numerical results [11] and wind tunnel data for the propelled Goldschmied airship with a freestream Mach number of 0.21.

Table 4. Total Propulsor Pressure and Velocity Ratios for Zero Wake Drag Coefficient for propelled Goldschmied Propulsor at M_∞=0.21

	Goldschmied WT [4]	Numerical Results [11]	Present Results USM3D – SA
Po_{jet}/P_∞	1.02	1.052	1.053
U_{jet}/U_∞	0.675	1.042	1.043

The present numerical results compared well with numerical results [11] and wind tunnel data [2, 4] for all three configurations. The wake drag coefficient as computed by the SA and SST turbulence models bracketed the wind tunnel data [2]. The next step was to use the developed tools and methodology to design an experiment to optimize the inlet slot to jet outlet area ratio in order to maximize the benefit of BLI on an aircraft fuselage. The XZS2G-1 airship, the Cerrata

BLC airship, and the Goldchmied propulsor were used to validate the computational tools however the emphasis of this study is aircraft BLI.

IV. Design of Experiment

At the start of this study, a baseline geometry was selected as a point of comparison for the BLI geometries. The selected baseline was a fuselage similar to a Boeing 737-800. The 737-800 geometry was adjusted to make an axisymmetric version of the fuselage in order to enable the CFD to be run quasi-2D for faster function evaluations.

Four different BLI configurations were investigated. The first configuration was to simply take the baseline geometry and add an inlet slot just aft of the aft pressure bulkhead of the fuselage cabin in order to minimize the impact on the structure and the passenger cabin payload volume. This configuration was named "Baseline BLI". It was found that the suction from the inlet generated a low pressure in front of the inlet. Since the slot is on the tapered portion of the fuselage, this low pressure, on an aft facing surface, generates a force component in the drag direction. These realizations lead to the second configuration.

The second configuration is similar to the first, but the fuselage maintains baseline curvature (diameter) until the inlet slot. Aft of the inlet slot, the fuselage begins to taper back into the tail cone. This configuration was named "Constant Diameter". The third configuration is similar to the baseline, but with the addition of a tail boom that extends out behind the back of the fuselage. This configuration was named "Stingray," like the sea creature with the long tail. The intent was to keep all of the BLI ducting located behind the aircraft's tails. The fourth configuration is much like a modern submarine with the ducted propulsor at the aft end of the body and hence was called the "Submarine" configuration. Schematics of all four geometries are shown in Figure 12. The red line in Figure 12 shows the location of the inlet slot.

Bookkeeping of thrust versus drag becomes more difficult with BLI. Rather than attempt to bookkeep drag separate from thrust, it was decided to simply iterate on the jet pressure ratio, Po_{jet}/P_{∞}, of the BLI propulsor until the net axial force became zero. It was assumed that the ram drag of the inlet would be negligible due to the low momentum of the flow in the boundary layer and the inlet was not included in the iteration to achieve zero net axial force. Screening tests were performed and it was found that the inlet and exit areas were the variables that had the strongest impact on Po_{jet}/P_{∞} required to achieve zero net axial force. The two design variables selected for the experiment were therefore the inlet area and the inlet to exit area ratio. Using these two variables a face-centered design was selected. Figure 13 shows a graphic of the variable values tested.

Each computational analysis started by prescribing two initial values of Po_{jet}/P_{∞} and computing corresponding axial force. Typically each case ran for 50,000 iterations; the first 10,000 iteration ran as first order and then USM3D automatically switched to second order for 40,000 iterations. A new value for Po_{jet}/P_{∞} was then computed using equation (2). Using the new value for Po_{jet}/P_{∞}, the simulation continued by running for another 40,000 iterations and a new value of axial force was computed. This iterative process continued until jet thrust matched body skin friction and pressure force; i.e. a net axial force equal to zero on the body was achieved. Typically a total of four CFD function evaluations were needed before axial force of zero was achieved. Numerical calculations were conducted on the Westmere processors of NAS high performance computers. Each numerical experiment took approximately 2 clock hours using one node with 12 processors. Figure 14 shows a typical convergence for the numerical simulation.

V. Results and Discussion

The sensitivity analysis consisted of two sets of numerical calculations. One for a M_∞ = 0.3 and the second for M_∞ = 0.75. Flow analyses were conducted on the Baseline BLI (BBLI), Constant Diameter (CD), and Submarine (Sub) Fuselage Type configurations. It was found that the "Stingray" configuration did not provide sufficient volume to fix the required inlet and exit area, and thus was not run through the CFD. As stated earlier, the two design variables chosen for the sensitivity analysis study were inlet area and inlet to exit area ratio. For each configuration, eight or nine different variations of inlet area and inlet to exit area ratio as shown in Figure 13. A total of 112 test points grouped in 54 test runs were performed to match test points. The simulations started by prescribing two initial values of Po_{jet}/P_∞ and stopped once a value of Po_{jet}/P_∞ reached a value where the net axial force became zero. For the BBLI and CD configurations, steady Reynolds averaged Navier Stokes (RANS) simulations were conducted. Flow around the Sub configurations showed unsteadiness and hence those calculations were performed as an unsteady RANS simulation. All simulations were conducted with the assumption that the configurations are flying at an altitude of 30,000 ft. Table 5 shows the computed results for all four configurations for M_∞ = 0.3, while Table 6 shows the results for M_∞ = 0.75. Figure 14 shows typical convergence for one of the test cases.

Table 5. Results for Numerical Simulations at M_∞ = 0.3 and an altitude of 30,000 ft.

Geometry	Inlet Slot Width (ft)	Inlet Area (ft^2)	Inlet/Exit Area Ratio	Exit Area (ft^2)	Fx-$_{JET}$ (lbs)	M_{JET}	U_{JET} (ft/sec)	Po_{jet}/P_∞	$\dot{m}$ (slugs/sec)	Power Required (lb-ft/sec)	Power Savings
Baseline										116,181	
BBLI 1	1	30.3	1.01	30.020	488.1	0.09	89.39	1.02	2.37	43,633	62%
BBLI 2	1.5	45.03	0.99	45.340	529.0	0.07	72.75	1.01	2.89	38,485	67%
BBLI 3	1.25	37.68	1.37	27.470	504.0	0.10	99.88	1.02	2.42	50,342	57%
BBLI 4	1	30.3	1.49	20.379	476.1	0.12	119.97	1.03	2.16	57,114	51%
BBLI 5	0.75	23.01	1.34	17.190	462.4	0.13	134.09	1.03	2.04	62,006	47%
BBLI 6	0.5	15.28	1.00	15.207	457.3	0.15	145.40	1.03	1.96	66,488	43%
BBLI 7	0.75	23.01	0.65	35.374	532.6	0.09	86.33	1.02	2.69	45,982	60%
BBLI 8	1	30.3	0.50	60.745	603.0	0.07	67.86	1.01	3.62	40,918	65%
BBLI 9	1.25	37.68	0.65	58.184	590.8	0.07	68.68	1.01	3.51	40,577	65%
CD1	0.75	30	1.00	30.088	397.2	0.08	78.24	1.02	2.07	31,078.9	73%
CD 2	1	40	1.01	39.800	439.9	0.07	66.19	1.01	2.32	29,114.8	75%
CD 3	1	40	1.33	30.088		--	-	-	-		
CD 4	0.75	30	1.46	20.545	373.5	0.11	105.10	1.02	1.90	39,250.8	66%
CD 5	0.5	20	1.14	17.580	344.2	0.11	112.48	1.02	1.74	38,713.9	67%
CD 6	0.5	20	0.97	20.545	350.4	0.10	99.39	1.02	1.80	34,825.6	70%
CD 7	0.5	20	0.64	31.200	379.0	0.07	72.26	1.02	1.98	27,385.8	76%
CD 8	0.75	30	0.50	59.550	462.6	0.05	48.03	1.01	2.50	22,218.3	81%
CD 9	1	40	0.65	61.281	481.2	0.05	49.15	1.01	2.65	23,649.3	80%
Sub 1		29.66	0.99	29.907	306.5	0.10	99.68	1.01	2.61	30,550.2	74%
Sub 2		40	0.99	40.280	229.1	0.08	84.40	1.00	2.96	19,337.0	83%
Sub 3		37.07	1.31	28.395	354.1	0.13	127.03	1.01	3.14	44,982.3	61%
Sub 4		30	1.43	21.015	395.9	0.15	145.62	1.02	2.67	57,643.2	50%
Sub 5		22.93	1.30	17.668	394.1	0.14	142.72	1.02	2.21	56,249.4	52%
Sub 6		20	0.99	20.300	370.8	0.13	128.31	1.02	2.28	47,580.3	59%
Sub 7		22.93	0.66	34.680	423.8	0.13	128.86	1.01	3.86	54,613.3	53%
Sub 8		30	0.52	57.447	681.8	0.14	143.92	1.00	7.10	98,119.8	16%

BBLI = Baseline Boundary Layer Ingestion Configuration, CD = Constant Diameter Configuration, Sub = Submarine Configuration

The power reported in Tables 5 and 6, for BBLI, CD, and Sub Configurations was calculated as the product of jet thrust and the jet velocity. The power for the baseline configuration was computed as the product of axial force and freestream velocity. For the BBLI configuration, BBLI 6 had the least amount of jet thrust but lowest power savings. BBLI 6 corresponds to the design point with the smallest inlet slot and an inlet to exit area ratio of 1. BBLI 2 had the highest power savings of all BBLI configurations. BBLI 2 has an inlet slot width of 1 ft and inlet to exit area ratio of 1. For the CD configuration, CD 5 had the least amount of jet thrust and CD 8 had the highest power savings among all CD configurations. CD 8 is the configuration with the smallest inlet to exit area ratio. For the Sub configuration, Sub 2 had the least amount of jet thrust and had the highest power savings of all 27 configurations tested at M_∞ = 0.3. Similar behavior was found with a freestream Mach number of 0.75. Sub 2 configuration had the highest power savings with the least amount of jet thrust as shown in Table 6. The corresponding mass flow rate was 7.19 slugs/sec. The jet exit velocities and jet total pressures were lower than freestream values. Highlighted in light green are the cases which generated the least amount of jet thrust. While rows highlighted in light blue are test cases with the highest power savings.

Table 6. Results for Numerical Simulations at M_∞ = 0.75 and an altitude of 30,000 ft.

Geometry	Inlet Slot Width (ft)	Inlet Area (ft^2)	Inlet/Exit Area Ratio	Exit Area (ft^2)	Fx-$_{JET}$ (lbs)	M_{JET}	U_{JET} (ft/sec)	Po_{jet}/P_∞	$\dot{m}$ (slugs/sec)	Power Required (lb-ft/sec)	Power Savings
Baseline										1,568,569	
BBLI 1	1	30.3	1.01	30.020	3037.4	0.19	193.56	1.13	5.51	587,908.5	63%
BBLI 2	1.5	45.03	0.99	45.340	3414.3	0.16	160.56	1.10	6.75	548,204.2	65%
BBLI 3	1.25	37.68	1.37	27.470	3030.7	0.21	208.07	1.14	5.44	630,598.0	60%
BBLI 4	1	30.3	1.49	20.379	2767.2	0.25	247.96	1.17	4.85	686,152.1	56%
BBLI 5	0.75	23.01	1.34	17.190	2610.2	0.28	275.37	1.18	4.55	718,772.1	54%
BBLI 6	0.5	15.28	1.00	15.207	2497.6	0.30	295.10	1.19	4.32	737,021.4	53%
BBLI 7	0.75	23.01	0.65	35.374	3084.9	0.17	171.88	1.12	5.72	530,228.1	66%
BBLI 8	1	30.3	0.50	60.745	3530.1	0.14	136.90	1.8	7.65	483,446	69%
BBLI 9	1.25	37.68	0.65	58.184	3558.1	0.14	141.23	1.08	7.58	502,520.3	68%
CD1	0.75	30	1.00	30.088	2129.8	0.15	149.19	1.10	4.18	317,743.0	80%
CD 2	1	40	1.01	39.800	2497.5	0.13	126.16	1.09	4.66	315,090.3	80%
CD 3	1	40	1.33	30.088							
CD 4	0.75	30	1.46	20.545	1924.1	0.21	205.88	1.12	3.95	396,135.7	75%
CD 5	0.5	20	1.14	17.580	1833.5	0.24	235.51	1.12	3.86	431,807.7	72%
CD 6	0.5	20	0.97	20.545	1897.8	0.21	207.32	1.11	3.97	393,450.0	75%
CD 7	0.5	20	0.64	31.200	2162.4	0.15	151.69	1.09	4.39	328,016.7	79%
CD 8	0.75	30	0.50	59.550	2644.7	0.09	87.91	1.06	4.77	232,494.9	85%
CD 9	1	40	0.65	61.281	2833.3	0.09	91.46	1.07	5.14	259,135.8	83%
Sub 1		29.66	0.99	29.907	1738.7	0.24	237.64	1.05	6.26	413,171.9	74%
Sub 2		40	0.99	40.280	1123.6	0.21	207.66	1.01	7.19	233,314.7	85%
Sub 3		37.07	1.31	28.395	1545.4	0.30	299.88	1.03	7.18	463,436.0	70%
Sub 4		30	1.43	21.015	1914.2	0.35	345.72	1.06	6.22	661,790.2	58%
Sub 5		22.93	1.30	17.668	2018.8	0.33	331.40	1.10	5.20	669,016.5	57%
Sub 6		20	0.99	20.300	1879.8	0.28	276.75	1.09	5.05	520,237.1	67%
Sub 7		22.93	0.66	34.680	2105.6	0.30	300.74	1.04	8.80	633,232.9	60%
Sub 8		37.07	0.66	55.838	3999.08	0.38	376.53	1.02	17.5	1,503,878	4%

BBLI = Baseline Boundary Layer Ingestion Configuration, CD = Constant Diameter Configuration, Sub = Submarine Configuration.

VI. Summary and Conclusions

A numerical assessment of the performance of fuselage boundary layer ingestion propulsion was conducted. This study is an initial investigation into coupling the aerodynamics of the fuselage with a BLI propulsion system in order to determine if there is sufficient potential to warrant further investigation of this topic. At the onset of this work, numerical simulations of flow around the XZS2G-1 airship, Cerreta BLC airship, and Goldschmied propulsor were performed. The computed results showed good agreement with wind tunnel data and previous numerical results. The computational results proved the validity of BLI concept and provided incentive to further investigate BLI concepts.

The fuselage was then selected as the part of the aircraft to apply BLI propulsion concepts. A fuselage similar to a Boeing 737-800 was selected as a baseline geometry. Four different configurations were studied that are modifications to the 737-800 fuselage, the Baseline BLI configuration, the Constant diameter configuration, the Stingray configuration, and the Submarine configuration. All configurations were axisymmetric bodies of revolution with angle-of-attack set to zero. The inlet area and inlet-to-exit area ratio were chosen as the two key parameters in the sensitivity analysis study. Eight or nine test points were selected for each configuration. The Stingray configuration was not considered in the sensitivity analysis study because it didn't have sufficient volume to package the BLI. A sensitivity analysis study was conducted for a freestream Mach number of 0.3 and 0.75

A total of 54 computational runs were conducted. Each run started with an initial guess for Po_{jet}/P_{∞} and then iterated on Po_{jet}/P_{∞} of the propulsor until the net axial force became zero. For all the configurations, the jet exit velocity was always lower than freestream velocity. The jet total pressure was also lower than the freestream value. Submarine configurations required the least amount of Po_{jet}/P_{∞}. Sub 2 and CD 8 gave the highest savings in power, with a power saving of 81-85% over the baseline configuration. However, since this study did not take into account the power needed to operate the BLI or the ram drag at the inlet, this is an optimistic result. This study was a conceptual level study of the physics behind BLI in order to design fuselages that maximize their BLI benefit. Results are encouraging, but a more detailed study needs to be conducted where the inlet ram drag, inlet shape optimization, internal ducting and power needed for the BLI propulsor are taken into account.

Acknowledgments

The authors would like to thank NASA Fixed Wing Project for funding this project. The authors would like to thank Dr. Khaled Abdol-Hamid at NASA Langley Research Center for his valuable comments and long hours of discussions and Dr. Mahogna Pandya for modifying USM3D output during the course of this work.

References

[1] Goldschmied, F. R., "Proposal for the study of Application of Boundary-Layer Control to Lighter-than-Air Craft", Goodyear Aircraft Corp., Rpt. GER-5796, 1954.

[2] P. A. Cerreta, "Wind-Tunnel Investigation of the Drag of Proposed Boundary-Layer-Controlled Airship," David Taylor Model Basin Aero Report 914, March 1957.

[3] F. R. Goldschmied, "Jet-propulsion of subsonic bodies with jet total-head equal to free stream's", AIAA Paper 1983-1790

[4] F. R. Goldschmied, "On the aerodynamic optimization of mini-RPV and small GA aircraft", AIAA Paper 1984-2163

[5] F. R. Goldschmied, "Aerodynamic design of low-speed aircraft with a NASA fuselage/wake-propeller configuration", AIAA Paper 1986-2693

[6] F. R. Goldschmied, "Wind Tunnel Tests of the Modified Goldschmied Model with Propulsion and Empennage: Analysis of Test Results," David W. Taylor Naval Ship R&D Center DTNSRDC-ASED-CR-02-86 FRG-82-1, February 1986.

[7] F. R. Goldschmied, "Fuselage self-propulsion by static-pressure thrust - Wind-tunnel verification", AIAA Paper 1987-2935.

[8] F. R. Goldschmied, “On a least-energy hypothesis for the wake of axisymmetric bodies with turbulent separation - Pressure-distribution prediction”, AIAA Paper 1988-2513.
[9] H. J. a. N. B. J. Howe, "An Experimental Evaluation of a Low Propulsive Power, Discrete Suction Concept Applied to an Axisymmetric Vehicle," David W. Taylor Naval Ship Research And Development Center DTNSRDC/TM-16-82/02, January 1982.
[10] P. N. Peraudo, J. A. Schetz, and C. J. Roy. "Computational Study of the Embedded Engine Static Pressure Thrust Propulsion System", Journal of Aircraft, Vol. 49, No. 6 (2012), pp. 2033-2045.
[11] M. Drela, "Power Balance in Aerodynamic Flows," AIAA Journal, vol. 47, no. 7, pp. 1761-1771, 2009.
[12] A. P. Plas, M. A. Sargeant, V. Madani, D. Crichton, E. M. Greitzer, T. P. Hynes, C. A. Hall “Performance of a Boundary Layer Ingesting (BLI) Propulsion System”, AIAA Paper 2007-450
[13] Daggett, D. L., Kawai, R., and Friedman, D., “Blended Wing Body Systems Studies: Boundary Layer Ingestion Inlets With Active Flow Control” NASA/CR-2003-212670.
[14] J. Roepke, K. Jameson, and M. Moore. “Upcoming Wind Tunnel Tests Investigating the Goldschmied Propulsor Concept”, AIAA Paper-201-6980. September 2011
[15] Roepke, Joshua, “An Investigation of a Goldschmied Propulsor,” Master’s Thesis, California Polytechnic State University, San Luis Obispo, 2012.
[16] Thomason, Nicole, “Experimental Investigation of Suction Geometry on a Goldschmied Propulsor,” Master’s Thesis, California Polytechnic State University, San Luis Obispo, 2012.
[17] Seubert, Cory “A Comparison of Computational Fluid Dynamic Results as Applied to California Polytechnic’s Goldschmied Propulsor Wind Tunnel Testing,” Master’s Thesis, California Polytechnic State University, San Luis Obispo, 2012.
[18] TetrUSS Web page: http://tetruss.larc.nasa.gov/usm3d/index.html, May 2013
[19] Samareh, J.: “GridTool, A Surface Modeling and Grid Generation Tool,” Proceedings of the Workshop on Surface Modeling, Grid Generation, and Related Issues in CFD Solutions, NASA CP–3291, May 9–11, 1995.
[20] Pirzadeh, S.: “Unstructured Viscous Grid Generation by Advancing-Layers Method,” AIAA Journal, Vol. 32, No. 8, pp. 1735–1737, August 1994.
[21] Pirzadeh, S.: “Structured Background Grids for Generation of Unstructured Grids by Advancing Front Method,” AIAA Journal, Vol. 31, No. 2, pp. 257–265, February 1993.
[22] Frink, N. T., Pirzadeh, S. Z., Parikh, P. C., Pandya, M. J., and Bhat, M. K.: “The NASA Tetrahedral Unstructured Software System,” The Aeronautical Journal, Vol. 104, No. 1040, October 2000, pp. 491-499.
[23] Frink, N. T.: “Assessment of an Unstructured-Grid Method for Predicting 3-D Turbulent Viscous Flows,” AIAA Paper-96-0292, January 1996.
[24] Pao, S. P.: “USMC6-TetrUSS Grid and Solution Cutter: A Brief Users’ Guide,” Version 4, NASA LaRC, September 2010.
[25] Nayani, S. and Campbell R., “Evaluation of Grid Modification Methods for On- and Off-Track Sonic Boom Analysis”, AIAA Paper 2013-798
[26] Abdol-Hamid, K. S., Frink, N. T., Deere, K. A., and Pandya, M. J.: “Propulsion Simulations Using Advanced Turbulence Models with the Unstructured-Grid CFD Tool, TetrUSS,” AIAA Paper 2004-0714, January 2004.
[27] Spalart P., and Allmaras S. A., “One-Equation Turbulence Model for Aerodynamic Flows,” AIAA Paper 92-0439, January 1992.
[28] Menter, F.R., “Improved Two-Equation k-omega Turbulence Models for Aerodynamic Flows,” NASA TM-103975, October 1992.
[29] Hartwich, P. M., and Frink, N. T., "Estimation of Propulsion-Induced Effects on Transonic Flows Over a Hypersonic Configuration" AIAA Paper 1992-0523
[30] Jones, B. M., “The measurement of profile drag by the pitot traverse method”, Aeronautical Research Council, Reports and Memoranda, 1688.

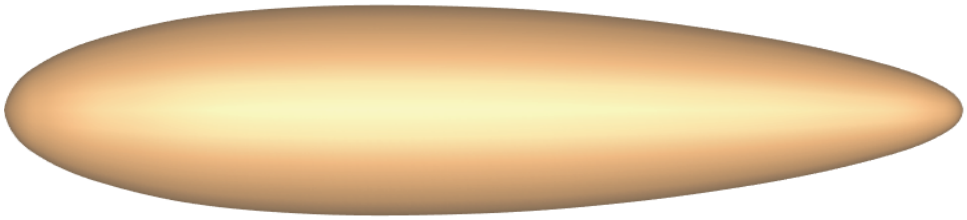

Figure 1. Schematic of the XZS2G-1 airship.

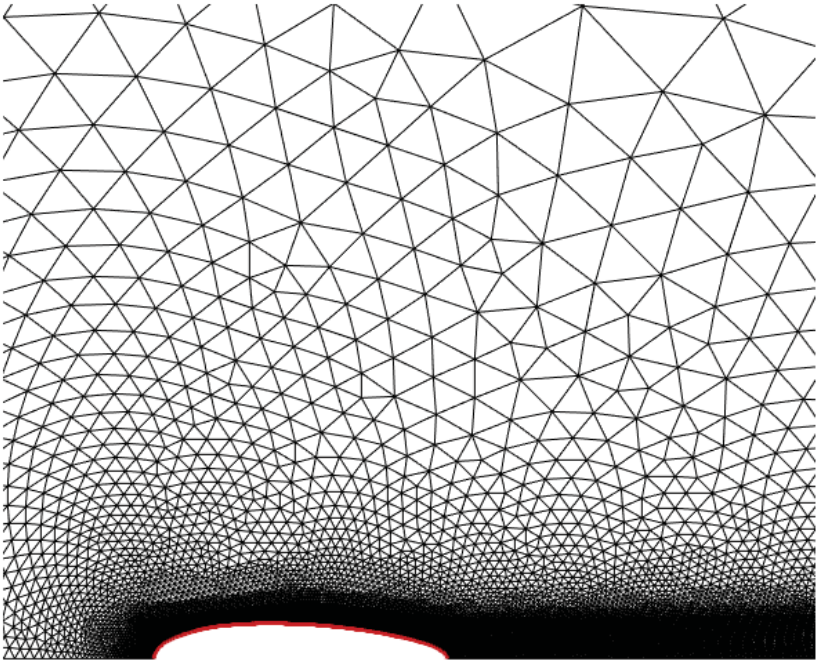

Figure 2. Planar cut showing the grid distribution for the XZS2G-1 airship.

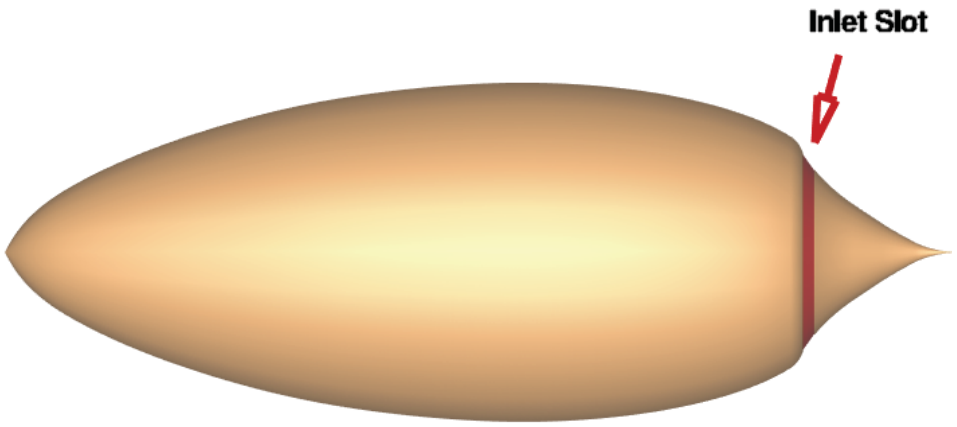

Figure 3. Schematic of the BLC airship. Red band illustrates location of suction gap.

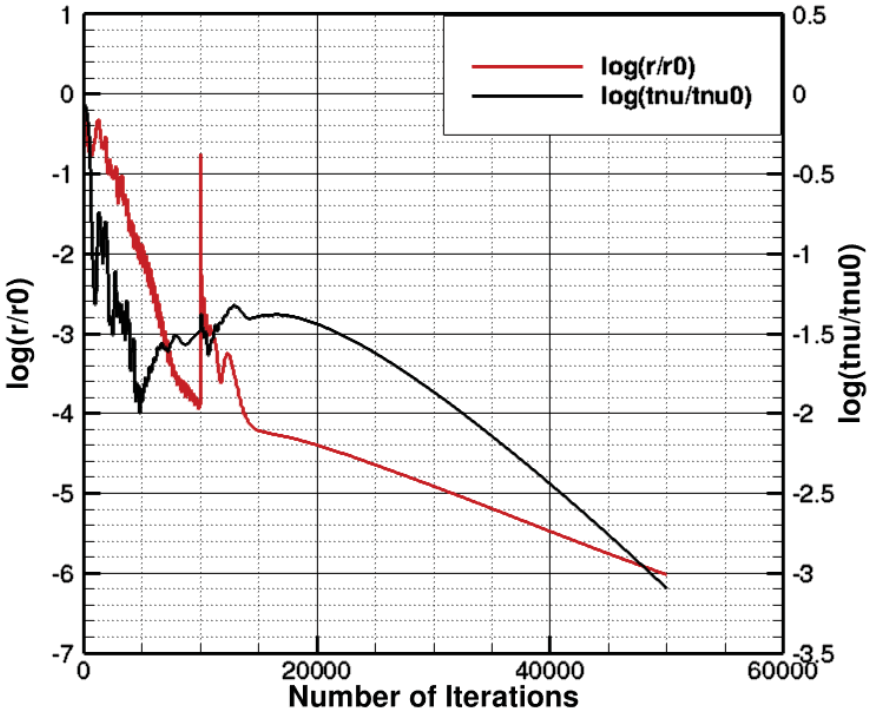

Figure 4. Convergence history for the BLC Airship at $M_\infty = 0.29$ and $Re_L = 10.2$ million.

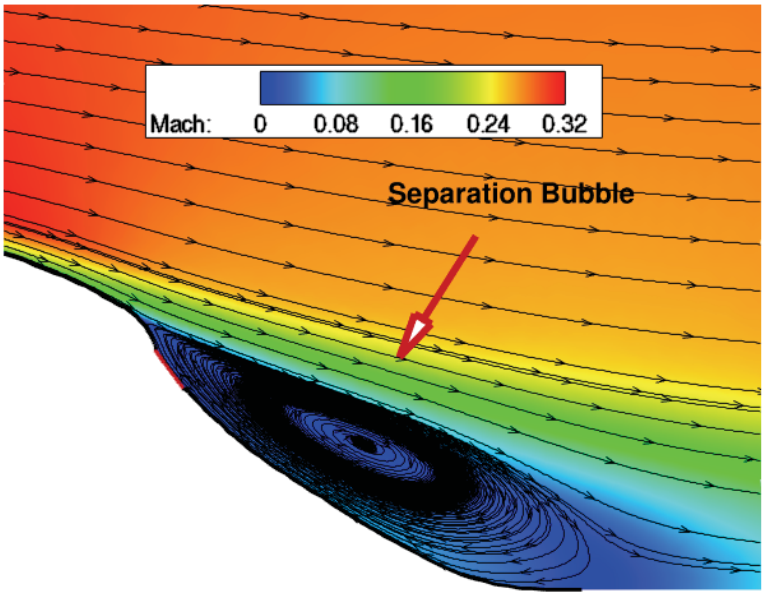

5a. No Suction

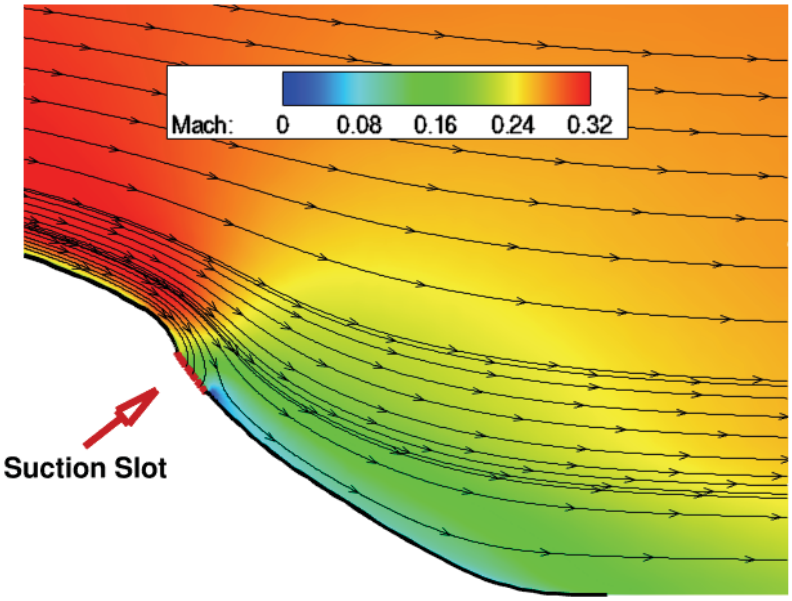

5b. Suction rate = 0.07 lb_f-sec/ft

Figure 5. Mach contours of the flow around tail of Cerreta Airship with streamlines superimposed at M_∞ = 0.29 and Re_L = 10.2 million.

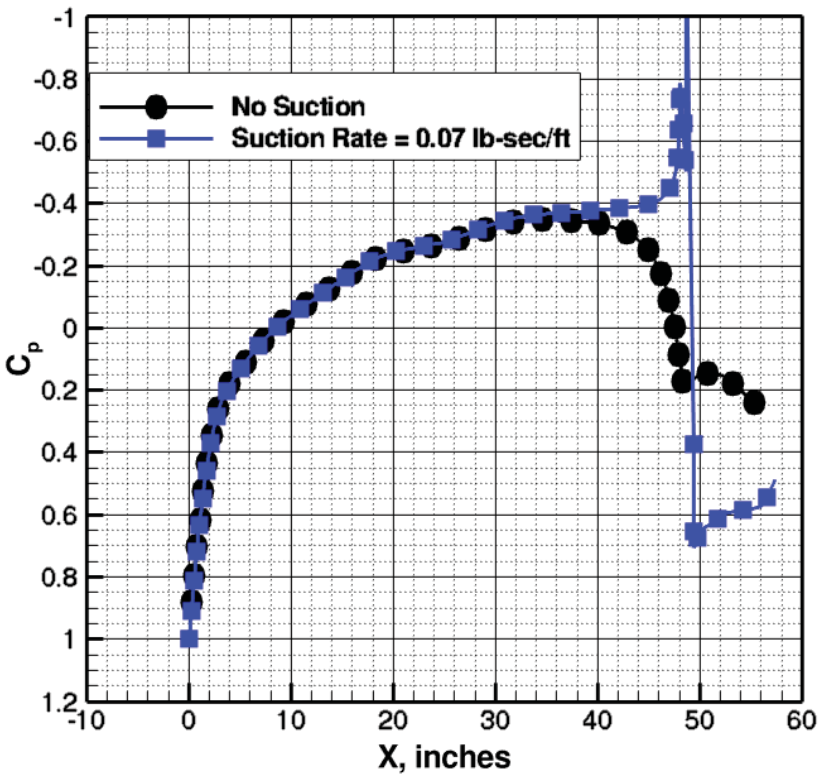

Figure 6. Computed pressure coefficients on the surface of Cerreta Airship at $M_\infty = 0.29$ and $Re_L = 10.2$ million.

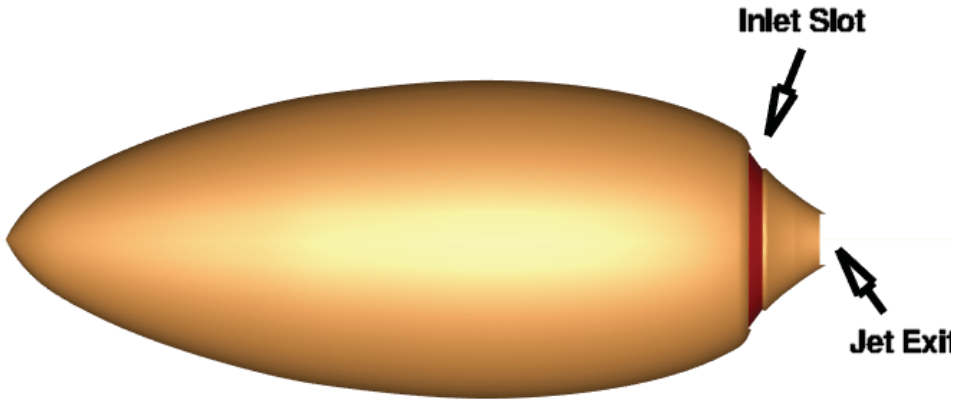

Figure 7. Schematic of Goldschmied propulsor. Red band illustrates location of suction gap.

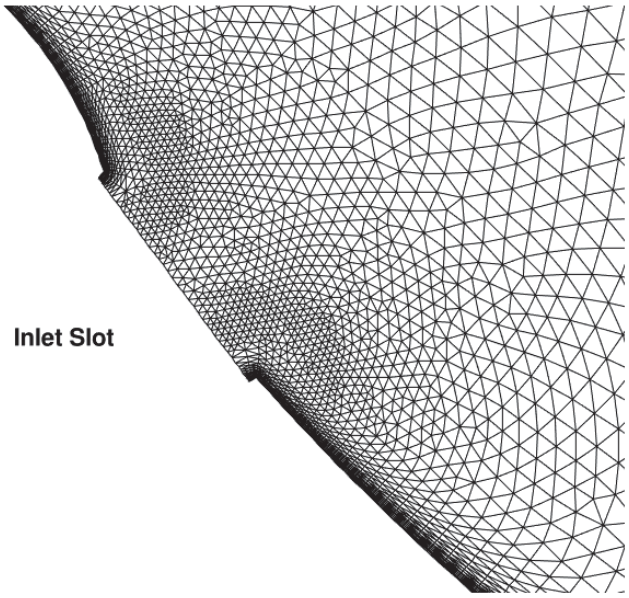

Figure 8. Grid distribution in the vicinity of the inlet slot for Goldschmied Propulsor.

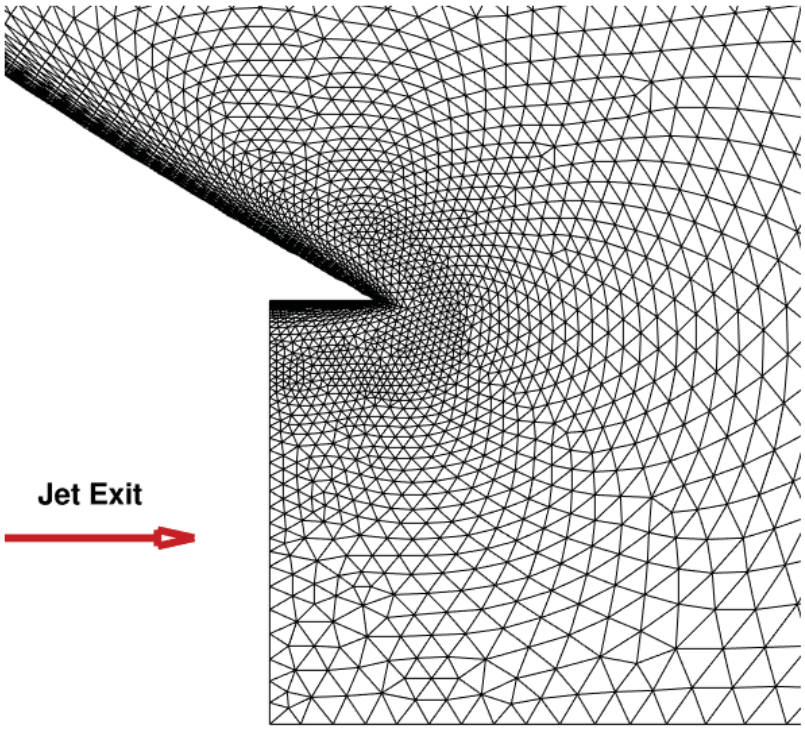

Figure 9. Grid distribution around jet exit for Goldschmied Propulsor.

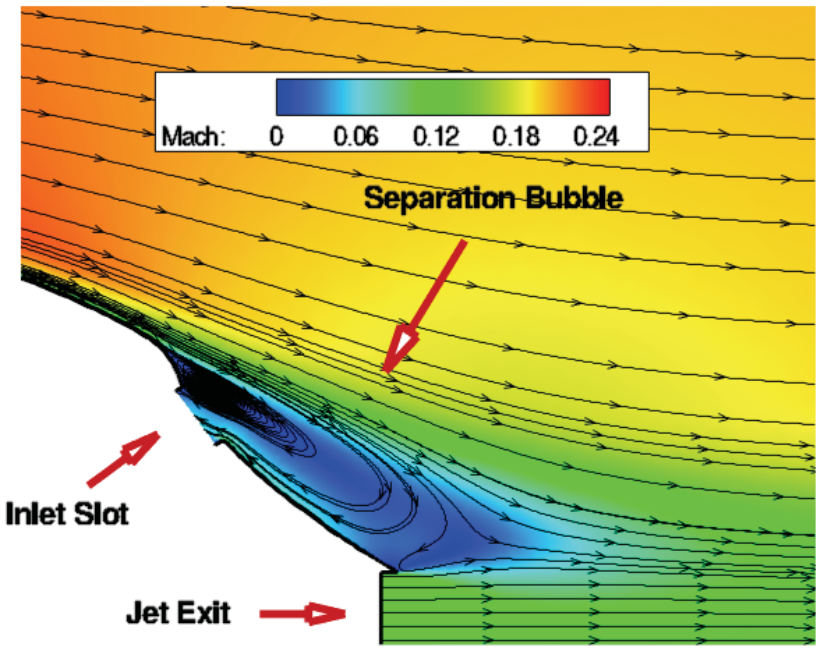

Figure 10. Mach contours of the flow around tail of Goldschmied Propulsor with streamlines superimposed at $M_\infty = 0.21$, $Re_L = 6.7$ million, and $Po_{jet}/P_\infty = 1.02$.

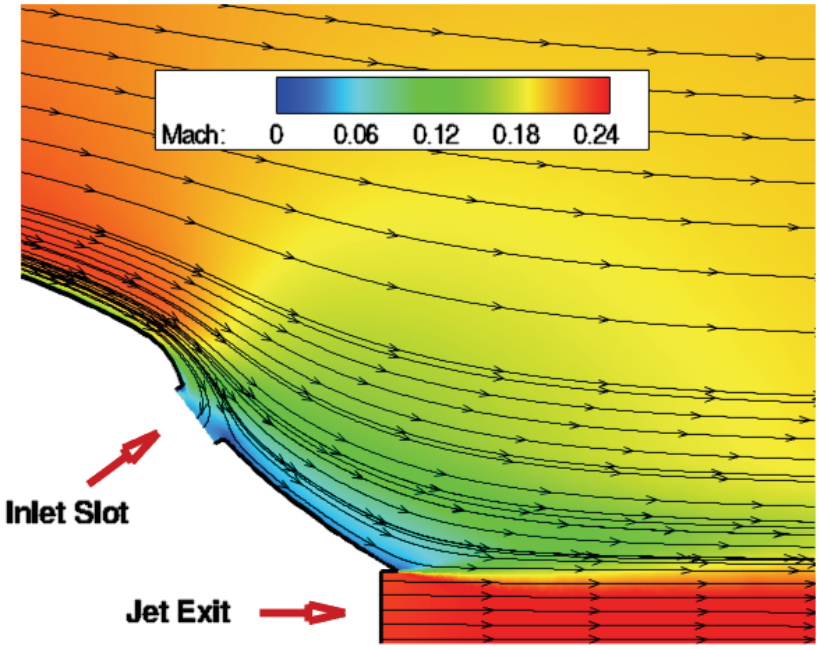

Figure 11. Mach contours of the flow around tail of Goldschmied Propulsor with streamlines superimposed at $M_\infty = 0.21$, $Re_L = 6.7$ million, and $Po_{jet}/P_\infty = 1.053$.

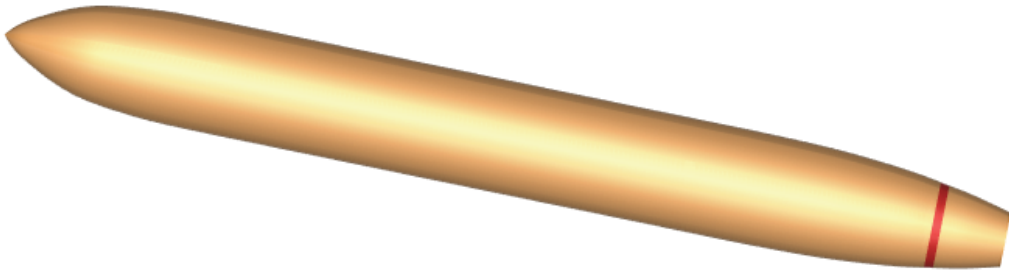

12a. Baseline BLI Configuration

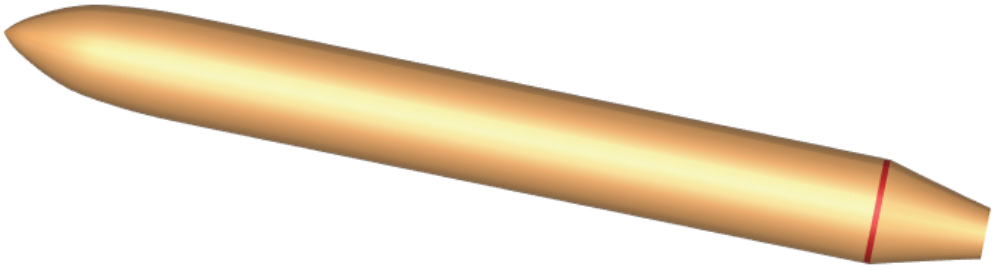

12b. Constant Diameter Configuration

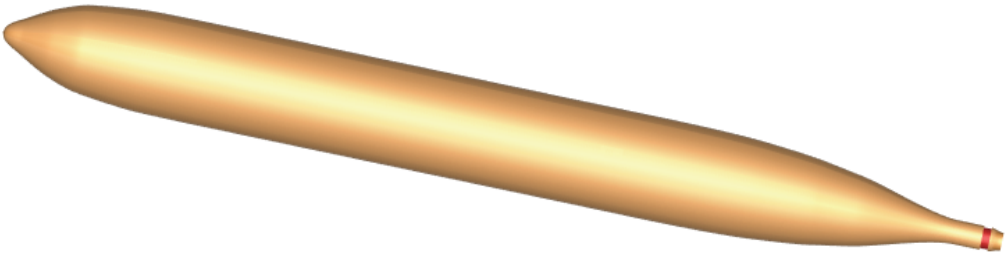

12c. Stingray Configuration

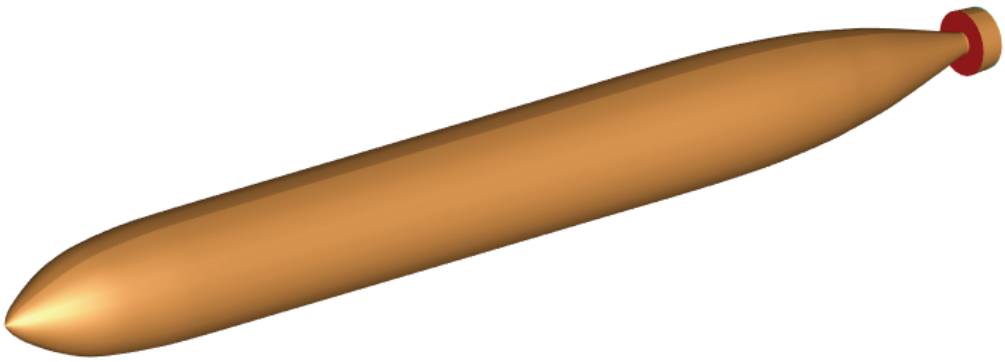

12d. Submarine Configuration

Figure 12. Schematic of BLI Configurations. Red band is location of inlet slot.

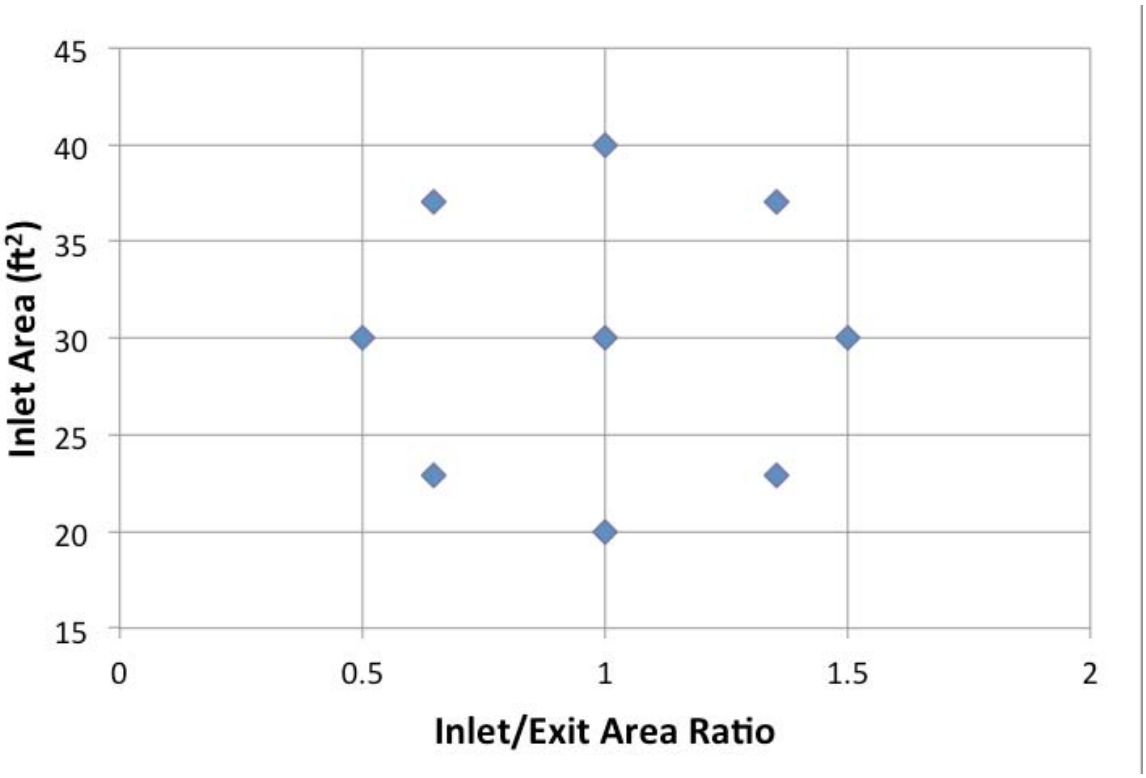

Figure 13. Central Composite Experiment Design.

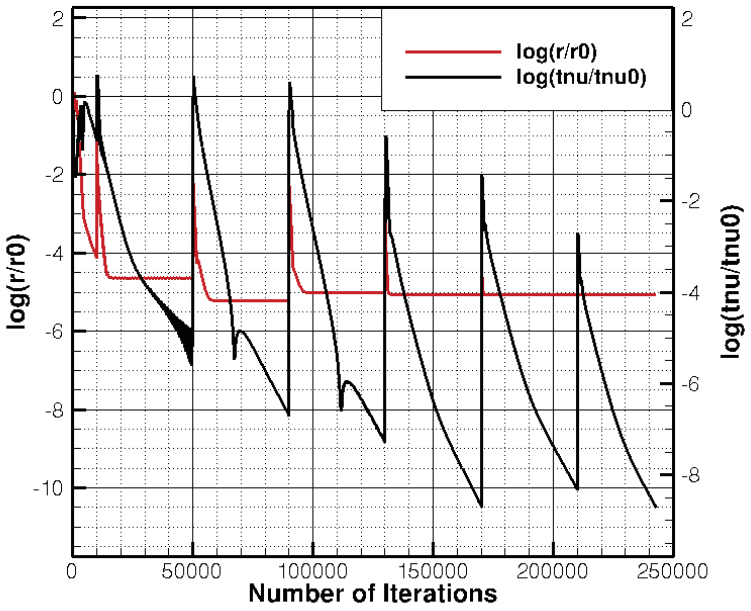

Figure 14. Convergence history for CD 1 configuration at $M_\infty = 0.75$ and $Re_L = 258$ million.